

Angular-spectrum-based analysis on the self-healing effect of Laguerre-Gaussian beams after an obstacle

Jian-Dong Zhang, Zi-Jing Zhang,^{*} Jun-Yan Hu,

Long-Zhu Cen, Yi-Fei Sun, Chen-Fei Jin,[†] and Yuan Zhao[‡]

School of Physics, Harbin Institute of Technology, Harbin 150001, China

(Dated: June 21, 2019)

Abstract

Self-healing, as an exotic effect, has showed many potential applications. In this paper, we focus on the self-healing effect of Laguerre-Gaussian beams after an obstacle. By taking advantage of angular spectrum theory, we study self-healing limit of the beam against on-axis obstacle. The dependence of self-healing capability on the radius of obstacle is analyzed. Additionally, we briefly discuss the self-healing limit of the beam in an off-axis scenario. Our results indicate that field amplitude of the beam will be healed well when the obstacle is approximately on-axis without oversized radius, perhaps providing advantages for optical communication, imaging, and remote sensing systems.

^{*} zhangzijing@hit.edu.cn

[†] jinchenfei@hit.edu.cn

[‡] zhaoyuan@hit.edu.cn

I. INTRODUCTION

Within the past two decades, the orbital angular momentum (OAM) of light [1] has developed rapidly and opened up a new avenue to a myriad of fields, such as quantum information processing [2–5], optical communications [6–9], and optical sensing [10–13]. Related to this, the methods for generation and measurement of OAM beams have gained a lot of attention. The conventional generation devices include cylindrical lenses [14], spiral phase plates [15], Q wave plates [16], and computational holograms [17]. The measurement methods are varied in comparison, besides reverse deploy of above generation devices, one can use interferometry [18–20], diffraction approach [21, 22], and geometric transformation [23–25].

Physically, OAM of the beams is associated with the Poynting vector which is not parallel to the direction of propagation. Mathematically, the beams carrying OAM—Laguerre-Gaussian (LG) and Bessel-Gaussian (BG) beams—are characterized by a spiral phase term of the form $\exp(i\ell\theta)$, where ℓ and θ are azimuthal mode index and coordinate, respectively. Different azimuthal modes are orthogonal and thus form an infinite-dimensional Hilbert space [26, 27], which provides a route to improve information capacity in a single photon. Furthermore, recent years have seen many studies on other exotic properties of OAM beams, diffraction-free behavior [28, 29], rotational Doppler effect [30–32], gradient force [33, 34], to name a few.

As one of these properties, self-healing effect of OAM beams [35–42] has been topical of late, as well as a fruitful testbed for conceptual or experimental demonstrations, optical communication [38], imaging [40], remote sensing [39], and so on [41, 42]. Of the previous studies, most aim to BG beams; by contrast, the study on LG beams is few and far between. As the paraxial approximate solutions of free-space Helmholtz equation in cylindrical coordinates, LG modes can be generated efficiently and have numerous applications. In addition, they show many unique properties and advantages when compared with BG beams. Therefore, the study on self-healing effect of LG beams is as important as that of BG beams. However, present studies have different opinions on who has better self-healing capability between LG and BG beams [35, 41]. This indicates that the related studies leave some gaps which need to bridge. To this end, here we address the self-healing effect of LG beams after an obstacle. Unlike previous protocols based upon intensity observation, we find a new way, angular spectrum theory, of analyzing this scenario.

The remainder of this paper is organized as follows. In Sec. II, we introduce the fundamental principle of self-healing effect. Section III gives the angular spectrum theory, and the self-healing capability of an LG beam after an on- or off-axis obstacle is studied. Finally, we summarize our work with a brief conclusion in Sec. IV.

II. FUNDAMENTAL PRINCIPLES

In what follows, we direct our attention to the schematic diagram of analysis on the self-healing effect, as shown in Fig. 1. An OAM beam carrying ℓ -fold spiral phase front is incident on an obstacle, an opaque disc inlaid in transparent glass. After a propagation distance z_1 , the beam is demodulated via a spiral phase plate (SPP) with reverse ℓ -fold phase structure. Finally, a CCD camera is placed at a distance of z_2 from the SPP to record intensity profile of the beam. In principle, without the obstacle, the intensity profile presented by the CCD camera obeys Gaussian distribution for a large enough z_2 . However, once the obstacle appears on the direction of propagation, the regularity of field amplitude is broken. Hand in hand with the amplitude destruction the beam starts repairing its field distribution. The primary task of this paper is to investigate the dependence of self-healing capability on the obstacle and propagation distance.

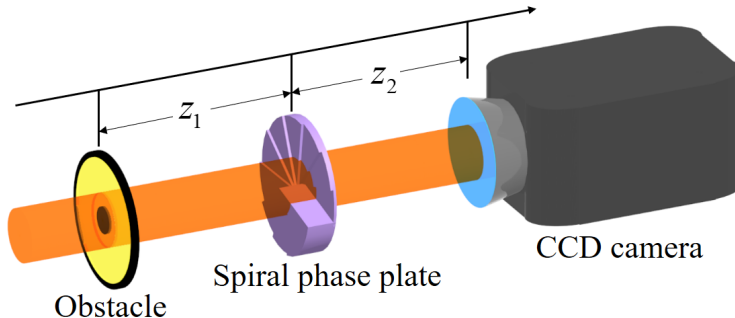


FIG. 1. Schematic diagram of analysis on the self-healing effect of LG beams.

Consider an LG beam as illumination input, of which the normalized field amplitude can be expressed as:

$$\begin{aligned}
 E_p^\ell(r, \theta, z) = & \frac{D_{\ell p}}{\omega} \left(\frac{\sqrt{2}r}{\omega} \right)^{|\ell|} L_p^{|\ell|} \left(\frac{2r^2}{\omega^2} \right) \exp \left(-\frac{r^2}{\omega^2} \right) \exp \left[\frac{ikr^2z}{2(z^2 + z_R^2)} \right] \\
 & \times \exp [-i(2p + |\ell| + 1)\phi] \exp (i\ell\theta), \tag{1}
 \end{aligned}$$

where r , θ , and z refer to cylindrical coordinates; $D_{\ell p} = \sqrt{2p!/\pi(p+|\ell|)!}$ is responsible for normalization; $\phi = \arctan(z/z_R)$ represents the Gouy phase; $z_R = k\omega_0^2/2$ is known as the Rayleigh range with wave vector k ; ω_0 and $\omega = \omega_0/\cos\phi$ are the beam waists at the beam focus and z plane, respectively; $L_p^{|\ell|}(\cdot)$ stand for the associated Laguerre polynomials with ℓ and p being the azimuthal and radial mode indices, respectively.

To such a field amplitude there corresponds a unique intensity profile with phase singularity, as illustrated in Fig. 2. Of most interest to us is the azimuthal mode index ℓ , which describes the number of phase jumps around the beam axis. Throughout this paper, we focus on the LG beams with $p = 0$ (doughnut beams [43]) as inputs.

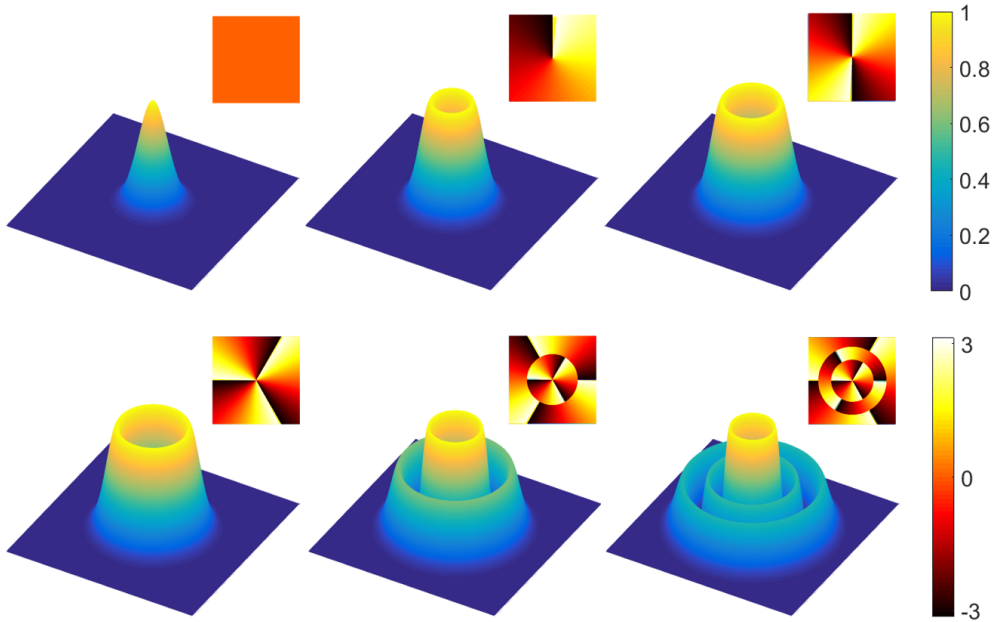


FIG. 2. Intensity profiles of LG beams in the initial plane ($z = 0$), where the upper right pattern in each inset is the corresponding phase front. The top and bottom color bars on the right correspond to the intensity profiles and phase fronts, respectively. The mode indices chosen in the figure (from left to right): top row, $p = 0$ and $\ell = 0, 1, 2$; bottom row, $\ell = 3$ and $p = 0, 1, 2$.

Regarding the obstacle, it can be considered as an amplitude-only device; accordingly, the transfer function is given by

$$O(r) = \begin{cases} 1, & r \leq r_0 \\ 0, & r > r_0 \end{cases} \quad (2)$$

with r_0 being radius of the opaque disc. It should be noted that, for an on-axis obstacle, an approximate expression without step functions can be used by the superposition of complex

Gaussian functions [44]. However, this approach is not adopted in this paper due to its intrinsic error along with error accumulation.

Upon leaving the obstacle, the output amplitude becomes $E_0(r, \theta, z) = E(r, \theta, z)O(r)$. For simplicity, here we consider the LG beam in the initial plane, i.e., $z = 0$. When the beam arrives at the SPP through free-space propagation, its amplitude can be calculated from Collins diffraction integral equation [45, 46]

$$E_1(r_1, \theta_1, z_1) = \frac{i}{\lambda z_1} \exp(-ikz_1) \int_0^{2\pi} \int_0^\infty E_0(r, \theta) \times \exp\left\{-\frac{ik}{2z_1} [r^2 - 2r_1r \cos(\theta_1 - \theta) + r_1^2]\right\} r dr d\theta, \quad (3)$$

where z_1 is the propagation distance.

The SPP is a phase-only device, of which the transfer function can be described as $S(\theta_1) = \exp(-i\ell\theta_1)$; consequently, the amplitude will go as $E'_1(r_1, \theta_1, z_1) = E_1(r_1, \theta_1, z_1) \exp(-i\ell\theta_1)$ when the beam passes through the SPP. The analogy of Eq. (3) gives beam amplitude at the plane of CCD camera,

$$E_2(r_2, \theta_2, z_2) = \frac{i}{\lambda z_2} \exp(-ikz_2) \int_0^{2\pi} \int_0^\infty E'_1(r_1, \theta_1, z_1) \times \exp\left\{-\frac{ik}{2z_2} [r_1^2 - 2r_2r_1 \cos(\theta_2 - \theta_1) + r_2^2]\right\} r_1 dr_1 d\theta_1. \quad (4)$$

Based on this amplitude expression, the self-healing effect can be analyzed.

III. RESULTS AND DISCUSSIONS

At the end of above section, the amplitude expression with overlap integral is given; however, it is by no means easy to free the amplitude expression from the integral. Owing to the difficulty in providing a mathematically tractable expression, in this section, we utilize numerical approach to analyze the self-healing effect. In Fig. 3, we show intensity profiles at the plane of CCD camera with different remainder intensity coefficients, W , and propagation distances, z_2 . The definition of remainder intensity coefficient is $W = \int_0^{2\pi} \int_0^\infty |E_0|^2 r dr d\theta / \int_0^{2\pi} \int_0^\infty |E|^2 r dr d\theta$ (see Appendix for derivation), where E and E_0 are the beam amplitudes before and after the obstacle, respectively.

It can be seen that intensity profiles converge towards Gaussian mode with the increase of propagation distance. By comparing with Figs. 3(a) and 3(b), one can also find that a high-order LG beam needs a larger propagation distance to approximately evolve into Gaussian

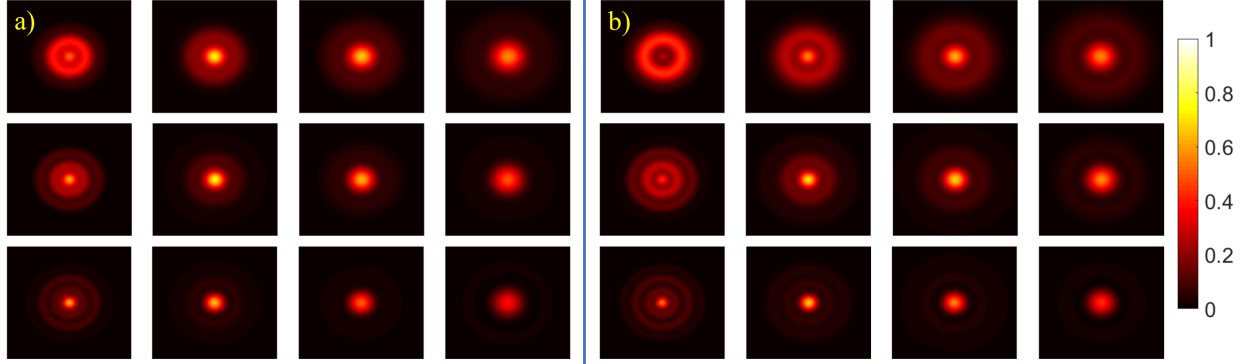


FIG. 3. (a) Intensity profiles at the plane of CCD camera against different remainder intensity coefficients, W , and propagation distances, z_2 , where $\ell = 2$, $z_1 = 0.4$ m, and $\omega_0 = \sqrt{\lambda/\pi}$ with wavelength $\lambda = 532$ nm. The dimensions of all subgraphs are $2 \text{ mm} \times 2 \text{ mm}$. From left to right: $z_2 = 0.5$ m, 1 m, 1.5 m, 2 m; from top to bottom: $W = 0.9, 0.7, 0.5$. (b) Same as group (a), but for $\ell = 3$. The color bar on the right holds true for each subgraph.

mode. For a small propagation distance, several rings appear in the outer region of the beam. These rings gradually blur as the beam continues to approach the plane of CCD camera. Regarding the same propagation distance, the multi-ring phenomenon becomes more obvious when decreasing remainder intensity coefficient, i.e., the increase of radius of obstacle. In addition, to accelerate the evolution of an OAM beam to Gaussian mode, one can add a lens after the SPP, or directly use a so-called vortex lens [47, 48] in place of the SPP.

In order to explain the origin of multi-ring phenomenon and explore the self-healing capability, we apply angular spectrum theory [49, 50] to analyze the self-healing effect of LG beams. According to this theory, the amplitude of an arbitrary OAM beam can be decomposed into LG modes, for different LG modes form an infinite-dimensional orthogonal basis. In this way, the amplitude after the obstacle can be written as:

$$E_0(r, \theta) = \frac{1}{\sqrt{2\pi}} \sum_{\ell} a_{\ell}(r) \exp(i\ell\theta), \quad (5)$$

where the weight factor can be obtained by the discrete Fourier relationship [51]

$$a_{\ell}(r) = \frac{1}{\sqrt{2\pi}} \int_0^{2\pi} E_0(r, \theta) \exp(-i\ell\theta) d\theta. \quad (6)$$

Further, we can determine the probability of finding a photon with an OAM of $\ell\hbar$ in the

beam after the obstacle,

$$P_\ell = \frac{C_\ell}{\sum_\ell C_\ell} \quad (7)$$

with $C_\ell = \int_0^\infty |a_\ell(r)|^2 r dr$. The self-healing capability refers to the degree to which the beam can maintain its original form. As a result, we take advantage of the normalized probability P_ℓ to delineate self-healing capability.

After angular spectrum calculation, we can find that the spectrum after an on-axis obstacle stays the same irrespective of the radius of obstacle, as depicted in Fig. 4. Meanwhile, a large radius of obstacle corresponds to obvious multi-ring phenomenon when compared with a small one. The physical reason behind these is the spread in spectrum resulting from the obstacle. On the one hand, the rotational symmetry of the obstacle prevents the changes in azimuthal indexes and further enforces angular spectrum conservation. On the other hand, due to the limitation in the radial direction, different radial modes will interact and change [26]. Based on the above statement, the field amplitude after the obstacle can be described as a superposition of LG modes,

$$E_1(r_1, \theta_1, z_1) = \sum_{p=0}^{\infty} \alpha_p E_p^\ell(r_1, \theta_1, z_1), \quad (8)$$

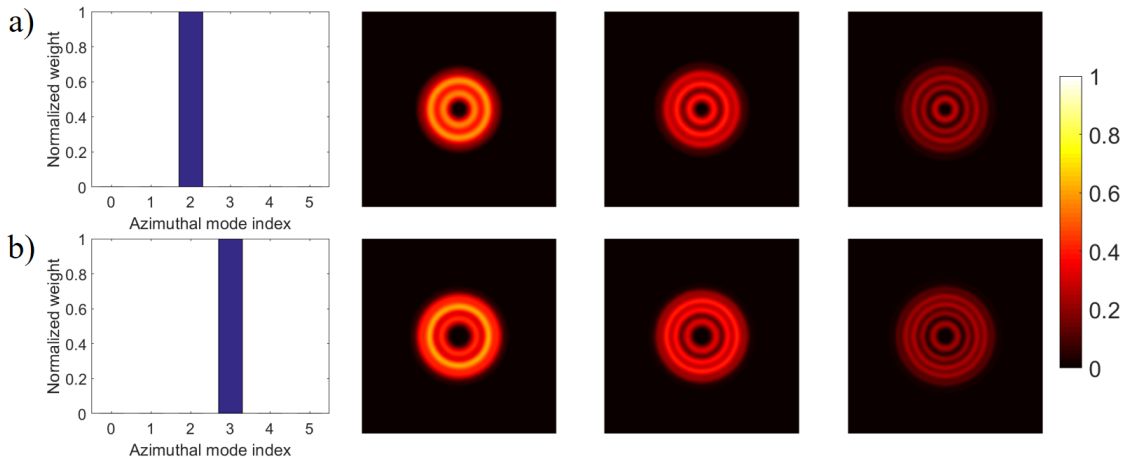


FIG. 4. (a) Angular spectra and intensity profiles before the SPP against different remainder intensity coefficients W , where $\ell = 2$, $z_1 = 0.4$ m, and $\omega_0 = \sqrt{\lambda/\pi}$ with wavelength $\lambda = 532$ nm. The dimensions of all intensity subgraphs are $2 \text{ mm} \times 2 \text{ mm}$. From left to right: $W = 0.9, 0.7, 0.5$. (b) Same as group (a), but for $\ell = 3$. The color bar on the right holds true for each subgraph of intensity profiles.

all with the same azimuthal index but a range of radial indices [52, 53].

With different propagation distances and radii taken, Fig. 5 shows the intensity profiles after the obstacle. The results suggest that either decreasing radius or increasing propagation distance can weaken the multi-ring phenomenon. This means that the field amplitude converge towards a nearly pure LG beam in the far field. Overall, however great the radius may be, an LG beam can always heal its broken field amplitude as the angular spectrum remains the same.

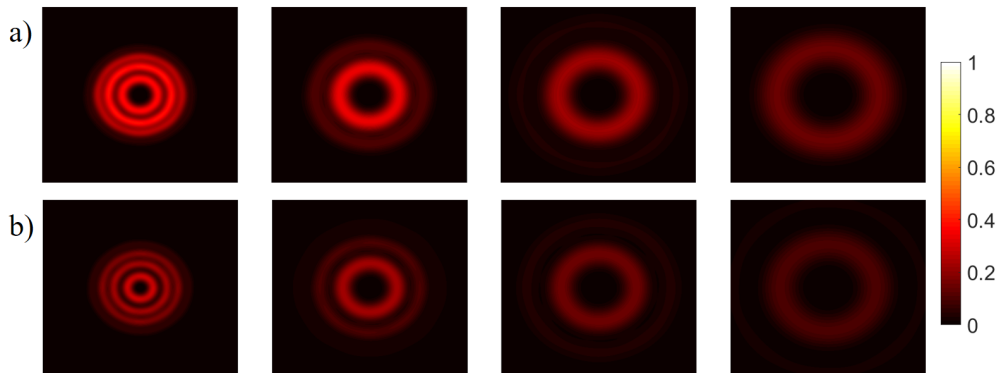


FIG. 5. (a) Intensity profiles after the obstacle against different propagation distances z_1 , where $\ell = 3$, $W = 0.7$, and $\omega_0 = \sqrt{\lambda/\pi}$ with wavelength $\lambda = 532$ nm. From left to right: $z_1 = 0.5$ m, 1 m, 1.5 m, 2 m. The dimensions of all subgraphs are $2 \text{ mm} \times 2 \text{ mm}$. (b) Same as group (a), but for $W = 0.5$. The color bar on the right holds true for each subgraph of intensity profiles.

Finally, we briefly discuss the self-healing capability in the presence of an off-axis obstacle. At this point, the transfer function of the obstacle is recast as:

$$O'(r) = \begin{cases} 1, & |r - \varepsilon| \leq r_0 \\ 0, & |r - \varepsilon| > r_0 \end{cases} \quad (9)$$

with an off-axis displacement ε , and other calculations are the same. Here the transfer function is labeled with a prime so as to distinguish it from that in on-axis scenario.

For an off-axis obstacle, it is invalid to simply define the remainder intensity coefficient, W . Hence, given a beam waist at the beam focus ω_0 , we introduce two dimensionless parameters as follows: radial coefficient $R_1 = r_0/\omega_0$, and displaced coefficients $R_2 = \varepsilon/\omega_0$.

Figure 6 gives the dependence of remainder weight, P_ℓ , on radial coefficient, R_1 , and displaced coefficient, R_2 . One can find that the effect of a small radial coefficient on spread in spectrum is always negligible ($P_\ell \approx 1$) regardless of displaced coefficient. Meanwhile, for a

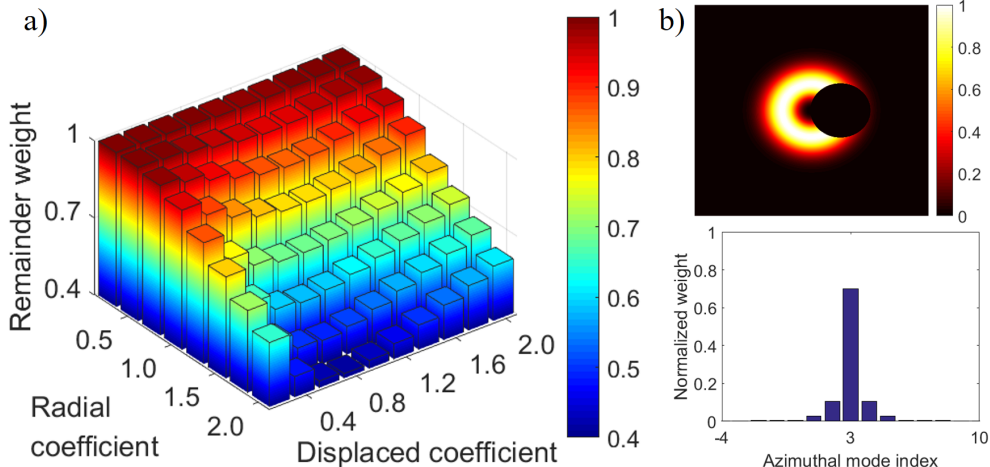


FIG. 6. (a) Remainder weights P_ℓ against different radial coefficients, R_1 , and displaced coefficients, R_2 , where $\ell = 3$ and $\omega_0 = \sqrt{\lambda/\pi}$ with wavelength $\lambda = 532$ nm. (b) Intensity profile and angular spectrum in the case of $R_1 = 1.25$ and $R_2 = 1.2$.

given radial coefficient, remainder weight is not a monotonic function of displaced coefficient. The most serious spread in spectrum will occur when a segment of the beam intensity is completely shielded, as shown in Fig. 6 (b). This originates from the maximum violation of rotational symmetry induced by the off-axis obstacle. In addition, when the obstacle is approximately on-axis ($R_2 \leq 0.2$) and its radius is not oversized ($r_0 \leq \omega_0$ or $R_1 \leq 1$), the remainder weight will be superior to 90%.

IV. CONCLUSIONS

In conclusion, we have studied the self-healing effect of LG beams. The self-healing limit of the beam is discussed through the use of angular spectrum analysis. Regarding to an on-axis obstacle, due to rotational symmetry, there is no spread in spectrum no matter what radius of the obstacle is. However, the interaction of radial modes becomes strong with the increase of radius; accordingly, non-zero radial mode cannot directly evolve into Gaussian mode. In addition, with a radius of the obstacle given, the interaction of radial modes can be weakened by increasing the azimuthal index. As to an off-axis obstacle, the weakest self-healing capability appear in the situation that a segment of the beam intensity is completely shielded. For an approximately on-axis obstacle with a not oversized radius, $R_2 \leq 0.2$ and $R_1 \leq 1$, an initial angular spectrum of the beam in excess of 90% can be well

maintained. These results may be useful for optical communication, imaging, and remote sensing systems.

ACKNOWLEDGMENT

This work was supported by the National Natural Science Foundation of China (Grant No. 61701139).

APPENDIX

In this section, we provide the calculation approach to remainder intensity coefficient after an on-axis obstacle. The result also applies to the scenario that an LG beam passes through an iris with a circular opening of radius r_0 .

First, one can verify that the field amplitude in Eq. (1) is normalized using the existing integral formula,

$$\int_0^{\infty} x^{2n+1} \exp(-bx^2) dx = \frac{n!}{2b^{n+1}} \quad (10)$$

That is, without any obstacles, the total intensity throughout space is 1. In addition, the specific expression of the associated Laguerre polynomial is found to be

$$L_p^\ell(x) = \sum_{k=0}^p (-1)^k \frac{(\ell+p)!}{k!(p-k)!(\ell+k)!} x^k. \quad (11)$$

It is obvious that the value of k takes on 0 under the constraint of $p = 0$; as a result, we have $L_p^\ell(x) = 1$ for each value of variable x . Further, the corresponding intensity distribution can be simplified as:

$$I_\ell(r, \theta, z) = |E_p^\ell(r, \theta, z)|^2 = \frac{2}{\pi |\ell|! \omega^2} \left(\frac{\sqrt{2}r}{\omega} \right)^{2|\ell|} \exp\left(-\frac{2r^2}{\omega^2}\right). \quad (12)$$

Based on this expression, the remainder intensity of the beam after the obstacle can be calculated from the following integral

$$W = 1 - 2\pi A \int_0^{r_0} r^{2|\ell|+1} \exp(-ar^2) dr \quad (13)$$

with $A = 2^{|\ell|+1}/(\pi\omega^{2+2|\ell|} |\ell|!)$ and $a = 2/\omega^2$. This can also be regarded as remainder intensity coefficient, for the input beam ahead of the obstacle is unit intensity.

Using the following integral formula,

$$\int x^n \exp(-bx^2) dx = -\frac{1}{2} \frac{1}{b^{(n+1)/2}} \Gamma\left(\frac{n+1}{2}, bx^2\right), \quad (14)$$

we get

$$\begin{aligned} W &= 1 + \frac{1}{2} \frac{1}{a^{(n+1)/2}} \left[\Gamma\left(\frac{n+1}{2}, ar_0^2\right) - \Gamma\left(\frac{n+1}{2}, 0\right) \right] \\ &= 1 + \frac{1}{2} \frac{1}{a^{(n+1)/2}} \left[\Gamma\left(\frac{n+1}{2}\right) - \int_0^{ar_0^2} t^{\frac{n+1}{2}-1} e^{-t} dt - \Gamma\left(\frac{n+1}{2}\right) \right] \\ &= 1 - \frac{1}{2} \frac{1}{a^{|\ell|+1}} \int_0^{ar_0^2} t^{|\ell|} e^{-t} dt. \end{aligned} \quad (15)$$

Here we take $n = 2|\ell| + 1$ and use the incomplete Gamma function and Gamma function

$$\Gamma(u, h) = \int_h^\infty t^{u-1} e^{-t} dt = \Gamma(u) - \int_0^h t^{u-1} e^{-t} dt, \quad (16)$$

$$\Gamma(u) = \int_0^\infty t^{u-1} e^{-t} dt = 2 \int_0^\infty t^{2u-1} \exp(-t^2) dt. \quad (17)$$

At this point, Eq. (15) can be rewritten as

$$W = 1 - \frac{1}{2} \frac{1}{a^{|\ell|+1}} \left[-e^{-f} \sum_{n=0}^{\ell} \frac{\ell! f^{\ell-n}}{(\ell-n)!} \right]_{f=0}^{f=ar_0^2} \quad (18)$$

with the integral formula

$$\int x^n e^{bx} dx = e^{bx} \sum_{k=0}^n (-1)^k \frac{n! x^{n-k}}{(n-k)! b^{k+1}}. \quad (19)$$

After some algebra, we obtain the expression of remainder intensity coefficient

$$W = \exp(-ar_0^2) \sum_{m=0}^{\ell} \frac{(ar_0^2)^{\ell-m}}{(\ell-m)!}. \quad (20)$$

This means that the integral in Eq. (13) is converted into an finite series, which is easy to calculate.

In Fig. 7 we show the remainder intensity coefficient W as a function of the radius r_0 of the obstacle with different mode indices. The result indicates that, for a given radius, a high-order LG beam corresponds to more intensity since it has a large dark area compared with a low-order one.

[1] L. Allen, M. W. Beijersbergen, R. J. C. Spreeuw, and J. P. Woerdman, *Phys. Rev. A* **45**, 8185 (1992).

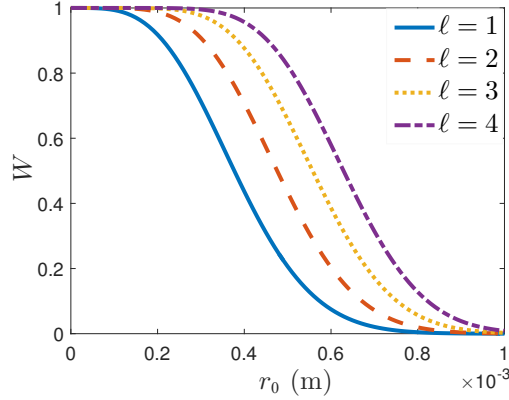


FIG. 7. The remainder intensity coefficient versus the radius r_0 of the obstacle, where $a = 2/\sqrt{\lambda/\pi}$ with wavelength $\lambda = 532$ nm.

- [2] Z.-Q. Zhou, Y.-L. Hua, X. Liu, G. Chen, J.-S. Xu, Y.-J. Han, C.-F. Li, and G.-C. Guo, *Phys. Rev. Lett.* **115**, 070502 (2015).
- [3] R. Fickler, R. Lapkiewicz, M. Huber, M. P. J. Lavery, M. J. Padgett, and A. Zeilinger, *Nat. Commun.* **5**, 4502 (2014).
- [4] S. K. Goyal, F. S. Roux, A. Forbes, and T. Konrad, *Phys. Rev. Lett.* **110**, 263602 (2013).
- [5] G. Puentes, N. Hermosa, and J. P. Torres, *Phys. Rev. Lett.* **109**, 040401 (2012).
- [6] W. Xi-Lin, C. Xin-Dong, S. Zu-En, C. Ming-Cheng, W. Dian, L. Li, L. Nai-Le, L. Chao-Yang, and P. Jian-Wei, *Nature* **518**, 516 (2015).
- [7] J. Wang, J. Y. Yang, I. M. Fazal, N. Ahmed, Y. Yan, H. Huang, Y. Ren, Y. Yue, S. Dolinar, and M. Tur, *Nat. Photon.* **6**, 488 (2012).
- [8] A. E. Willner, A. F. Molisch, C. Bao, G. Xie, H. Huang, J. Wang, L. Li, M. Tur, M. P. J. Lavery, and N. Ahmed, *Adv. Opt. Photon.* **7**, 66 (2015).
- [9] M. Krenn, J. Handsteiner, M. Fink, R. Fickler, R. Ursin, M. Malik, and A. Zeilinger, *Proc. Natl. Acad. Sci.* **113**, 13648 (2016).
- [10] J. Courtial, K. Dholakia, D. A. Robertson, L. Allen, and M. J. Padgett, *Phys. Rev. Lett.* **80**, 3217 (1998).
- [11] M. P. J. Lavery, F. C. Speirits, S. M. Barnett, and M. J. Padgett, *Science* **341**, 537 (2013).
- [12] O. S. Magaña Loaiza, M. Mirhosseini, B. Rodenburg, and R. W. Boyd, *Phys. Rev. Lett.* **112**, 200401 (2014).
- [13] J.-D. Zhang, C.-F. Jin, Z.-J. Zhang, L.-Z. Cen, J.-Y. Hu, and Y. Zhao, *Opt. Express* **26**,

- 33080 (2018).
- [14] M. Beijersbergen, L. Allen, H. van der Veen, and J. Woerdman, *Opt. Commun.* **96**, 123 (1993).
 - [15] G. Turnbull, D. Robertson, G. Smith, L. Allen, and M. Padgett, *Opt. Commun.* **127**, 183 (1996).
 - [16] L. Marrucci, C. Manzo, and D. Paparo, *Phys. Rev. Lett.* **96**, 163905 (2006).
 - [17] N. R. Heckenberg, R. McDuff, C. P. Smith, and A. G. White, *Opt. Lett.* **17**, 221 (1992).
 - [18] J. Leach, M. J. Padgett, S. M. Barnett, S. Franke-Arnold, and J. Courtial, *Phys. Rev. Lett.* **88**, 257901 (2002).
 - [19] W. Zhang, Q. Qi, J. Zhou, and L. Chen, *Phys. Rev. Lett.* **112**, 153601 (2014).
 - [20] J. Leach, J. Courtial, K. Skeldon, S. M. Barnett, S. Franke-Arnold, and M. J. Padgett, *Phys. Rev. Lett.* **92**, 013601 (2004).
 - [21] A. Mourka, J. Baumgartl, C. Shanor, K. Dholakia, and E. M. Wright, *Opt. Express* **19**, 5760 (2011).
 - [22] F. Eilenberger, K. Prater, S. Minardi, R. Geiss, U. Röpke, J. Kobelke, K. Schuster, H. Bartelt, S. Nolte, A. Tünnermann, and T. Pertsch, *Phys. Rev. X* **3**, 041031 (2013).
 - [23] G. C. G. Berkhout, M. P. J. Lavery, J. Courtial, M. W. Beijersbergen, and M. J. Padgett, *Phys. Rev. Lett.* **105**, 153601 (2010).
 - [24] M. Malik, M. Mirhosseini, M. P. J. Lavery, J. Leach, M. J. Padgett, and R. W. Boyd, *Nat. Commun.* **5**, 3115 (2013).
 - [25] J. Zhou, W. Zhang, and L. Chen, *Appl. Phys. Lett.* **108**, 8185 (2016).
 - [26] Z. Xiao, R. N. Lanning, M. Zhang, I. Novikova, E. E. Mikhailov, and J. P. Dowling, *Phys. Rev. A* **96**, 023829 (2017).
 - [27] F. Bouchard, N. H. Valencia, F. Brandt, R. Fickler, M. Huber, and M. Malik, *Opt. Express* **26**, 31925 (2018).
 - [28] D. McGloin and K. Dholakia, *Contemp. Phys.* **46**, 15 (2005).
 - [29] V. Belyi, A. Forbes, N. Kazak, N. Khilo, and P. Ropot, *Opt. Express* **18**, 1966 (2010).
 - [30] M. P. J. Lavery, F. C. Speirits, S. M. Barnett, and M. J. Padgett, *Science* **341**, 537 (2013).
 - [31] M. P. J. Lavery, S. M. Barnett, F. C. Speirits, and M. J. Padgett, *Optica* **1**, 1 (2014).
 - [32] W. Zhang, J. Gao, D. Zhang, Y. He, T. Xu, R. Fickler, and L. Chen, *Phys. Rev. Applied* **10**, 044014 (2018).

- [33] A. T. O’Neil, I. MacVicar, L. Allen, and M. J. Padgett, *Phys. Rev. Lett.* **88**, 053601 (2002).
- [34] V. Garcés-Chávez, D. McGloin, M. J. Padgett, W. Dultz, H. Schmitzer, and K. Dholakia, *Phys. Rev. Lett.* **91**, 093602 (2003).
- [35] J. Mendoza-Hernández, M. L. Arroyo-Carrasco, M. D. Iturbe-Castillo, and S. Chávez-Cerda, *Opt. Lett.* **40**, 3739 (2015).
- [36] I. A. Litvin, M. G. McLaren, and A. Forbes, *Opt. Commun.* **282**, 1078 (2009).
- [37] R. Rop, I. A. Litvin, and A. Forbes, *J. Opt.* **14**, 035702 (2012).
- [38] I. Nape, E. Otte, A. Vallés, C. Rosales-Guzmán, F. Cardano, C. Denz, and A. Forbes, *Opt. Express* **26**, 26946 (2018).
- [39] S. Fu, T. Wang, Z. Zhang, Y. Zhai, and C. Gao, *Opt. Express* **25**, 20098 (2017).
- [40] F. O. Fahrbach and A. Rohrbach, *Nat. Commun.* **3**, 632 (2012).
- [41] M. McLaren, T. Mhlanga, M. J. Padgett, F. S. Roux, and A. Forbes, *Nat. Commun.* **5**, 3248 (2014).
- [42] E. Otte, I. Nape, C. Rosales-Guzmán, A. Vallés, C. Denz, and A. Forbes, *Phys. Rev. A* **98**, 053818 (2018).
- [43] A. Nicolas, L. Veissier, L. Giner, E. Giacobino, D. Maxein, and J. Laurat, *Nat. Photon.* **8**, 234 (2013).
- [44] J. J. Wen and M. A. Breazeale, *J. Acoust. Soc. Am.* **83**, 1752 (1988).
- [45] S. A. Collins, *J. Opt. Soc. Am.* **60**, 1168 (1970).
- [46] Y. Yang, Y. Dong, C. Zhao, and Y. Cai, *Opt. Lett.* **38**, 5418 (2013).
- [47] J. Grover A. Swartzlander, *Opt. Lett.* **31**, 2042 (2006).
- [48] A. M. W. Tam, F. Fan, T. Du, W. Hu, W. Zhang, C. Zhao, X. Wang, K.-L. Ching, G. Li, H. Luo, V. G. Chigrinov, S. Wen, and H.-S. Kwok, *Phys. Rev. Applied* **7**, 034010 (2017).
- [49] L. Torner, J. P. Torres, and S. Carrasco, *Opt. Express* **13**, 873 (2005).
- [50] L. Chen, J. Lei, and J. Romero, *Light: Sci. Appl.* **3**, e153 (2014).
- [51] E. Yao, S. Franke-Arnold, J. Courtial, S. Barnett, and M. Padgett, *Opt. Express* **14**, 9071 (2006).
- [52] A. M. Yao and M. J. Padgett, *Adv. Opt. Photon.* **3**, 161 (2011).
- [53] M. R. Dennis, K. O’Holleran, and M. J. Padgett, *Prog. Opt.* **53**, 293 (2009).